Machine learning predictions for bending capacity of ECC-concrete composite beams hybrid reinforced with steel and FRP bars

Wenjie Ge[1], Feng Zhang[1], Yi Wang[1], Ashraf Ashour[2], Laiyong Luo[3], Linfeng Qiu[4], Shihu Fu[5], Dafu Cao[1*]

1. College of Civil Science and Engineering, Yangzhou University, Jiangsu Yangzhou 225127, China;

2. Department of Civil and Structural Engineering, University of Bradford, Bradford BD71DP, UK;

3. Jiangsu Yangjian Group Co., Ltd, Jiangsu Yangzhou 225002, China;

4. Nantong Construction Engineering Quality Supervision Station, Jiangsu Nantong 226000, China;

5. Yangzhou Jianwei Construction Engineering Testing Center Co., Ltd., Jiangsu Yangzhou 225002, China;

Abstract: This paper explores the development of the most suitable machine learning models for predicting the bending capacity of steel and FRP (Fiber Reinforced Ploymer) bars hybrid reinforced ECC (Engineered Cementitious Composites)-concrete composite beams. Five different machine learning models, namely Support Vector Regression (SVR), Extreme Gradient Boosting (XGBoost), Multilayer Perceptron (MLP), Random Forest (RF), and Extremely Randomized Trees (ERT), were employed. To train and evaluate these predictive models, the study utilized a database comprising 150 experimental data points from the literature on steel and FRP bars hybrid reinforced ECC-concrete composite beams. Additionally, Shapley Additive Explanations (SHAP) analysis was employed to assess the impact of input features on the prediction outcomes. Furthermore, based on the optimal model identified in the research, a graphical user interface (GUI) was designed to facilitate the analysis of the bending capacity of hybrid reinforced ECC-concrete composite beams in practical applications. The results indicate that the XGBoost algorithm exhibits high accuracy in predicting bending capacity, demonstrating the lowest root mean square error, mean absolute error, and mean absolute percentage error, as well as the highest coefficient of determination on the testing dataset among all models. SHAP analysis indicates that the equivalent reinforcement ratio, design strength of FRP bars, and height of beam cross-section are significant feature parameters, while the influence of the compressive strength of concrete is minimal. The predictive models and graphical user interface (GUI) developed can offer engineers and researchers with a reliable predictive method for the bending capacity of steel and FRP bars hybrid reinforced ECC-concrete composite beams.

Keywords: machine learning; bending capacity; ECC-concrete composite beams; hybrid reinforcement

1.Introduction

With the continuous advancement of construction engineering, there has been an increasing demand for the structural performance, challenging the traditional reinforced concrete (RC) structures to meet the requirements of bearing capacity, durability, and ductility [1]. Consequently, innovative materials and structural systems are being explored to enhance the performance and longevity of these structures.

Concrete, as the most widely used building material in modern times, holds particular significance in the construction industry worldwide [2]. However, with advancements in modern

structural engineering, traditional RC structures are required to not only meet high-performance criteria such as compressive and tensile strength but also exhibit qualities like durability and ductility. Thus, there is a necessity to seek a construction material with high ductility and durability.

In recent years, Engineered Cementitious Composites (ECC), proposed by Victor C Li of the University of Michigan, USA, have offered an effective solution to address the issues of excessive brittleness and wide cracks in RC structures [3]. ECC does not contain coarse aggregates like gravel, instead, it incorporates a suitable amount of short fibers as reinforcement material, constituting a composite material comprising an ultra-high ductile cementitious matrix and fibers [4]. Compared with concrete, ECC exhibits greater ductility and has the ability to deform and control crack widths effectively, demonstrating characteristics of multiple micro-cracking and strain hardening.

Fiber Reinforced Polymer (FRP) rebar is a composite material composed of continuous and binding fibers, offering advantages such as lightweight, high corrosion resistance, durability, and high tensile strength. It finds wide application in fields like bridge engineering and marine engineering [5-6]. However, the inherent drawbacks of FRP material include low elastic modulus, linear stress-strain relationship without yielding stage, and brittle failure mode, resulting in large deflections and crack widths in FRP RC structures during service, significantly affecting their normal functionality. This also limits the widespread application of FRP RC structures in civil engineering [7]. Qu et al. proposed combining fiber-reinforced polymer and steel reinforcement in reinforced concrete beams, concluding that this system provides higher strength, with FRP enhancing durability, while steel improving ductility [8-9]. Placing FRP rebar at corners and steel reinforcement internally, while using Engineered Cementitious Composites (ECC) to replace concrete in the tension zone of beams, improves the cracking, yielding, bearing capacity, and stiffness of flexural beams [10].

In recent years, the application of machine learning-based predictive models in civil engineering has garnered significant attention [11-12]. Particularly, establishing intelligent models to predict the mechanical and durability properties of construction materials is one of the most important innovative approaches in this field. This method offers the possibility of more detailed studies on structural behavior. Through predictive modeling, researchers can better correlate

structural performance with various parameters and gain a better understanding of their future performance.

Ahmet et al. [13] conducted machine learning predictions of the load capacity of 217 ECC reinforced concrete beams. The research findings indicate that the model developed using the Extreme Gradient Boosting (XGBoost) algorithm achieved an accuracy of over 80%. The most influential parameters include the compressive strength of the concrete substrate, beam height, longitudinal reinforcement ratio, and ECC thickness. Wakjira et al. [14] performed machine learning predictions of the load capacity of 132 FRP bars RC beams. They utilized six parameter indices and four machine learning algorithms. The results demonstrated that ensemble models based on boosting and tree-based methods (AdaBoost, GBDT, and XGBoost) exhibited higher prediction accuracy. Additionally, the predictive model's accuracy surpassed the load capacity calculation formulas provided in the US and Canadian standards for FRP bars RC structures. Xiong et al. [15] employed machine learning-based methods to predict the flexural capacity of a novel prefabricated MVFT steel-concrete composite girder. The impact of input parameters such as the distance between steel girder's Tensile Centroid (TC) and slab's Compressive Centroid (CC), the distance between steel girder's TC and its CC, the compressive area of steel girder was analyzed. Two machine learning models, BP neural network and Squares Support Vector (SVR) were used. The results showed that the ultimate strength predictions of 30 meters MVFT girder by BP model have the best accuracy.

Steel and FRP bars hybrid reinforced ECC-concrete composite beams represent a novel composite system, characterized by high bearing capacity, ductility, good resistance to deformation and cracks. However, there is no research on machine learning predictions for these steel and FRP bars hybrid reinforced ECC-concrete composite beams. Therefore, this study aims to investigate the prediction of bending capacity through machine learning using data extracted from relevant literature on 150 steel and FRP bars hybrid reinforced ECC-concrete composite beams. Eight parameter indices are selected as input variables for the prediction. Five different machine learning models are chosen to evaluate the bending capacity prediction and their capabilities are compared. A major significance of this study is the development of a Graphical User Interface (GUI) module for the model with the optimal prediction accuracy and performance, which facilitates the solution

of complex problems and expanding the interfaces for human interaction.

2. Data acquisition

After reviewing relevant articles [16-23] on steel and FRP bars hybrid reinforced ECC-concrete composite beams and conducting screening, 150 experimental data were obtained. Due to their better tensile strength, ECC replaced concrete from the bottom to the top, locating the ECC layer at the bottom of all beams. All beams were subjected to two-point bending test. The loading diagram and reinforcement details are shown in Fig. 1. The beams exhibited different parameters in terms of section dimensions, strength of concrete and ECC, strength of steel and FRP reinforcements, reinforcement ratio, and height ratio of ECC, with specific parameters as shown in Table 1.

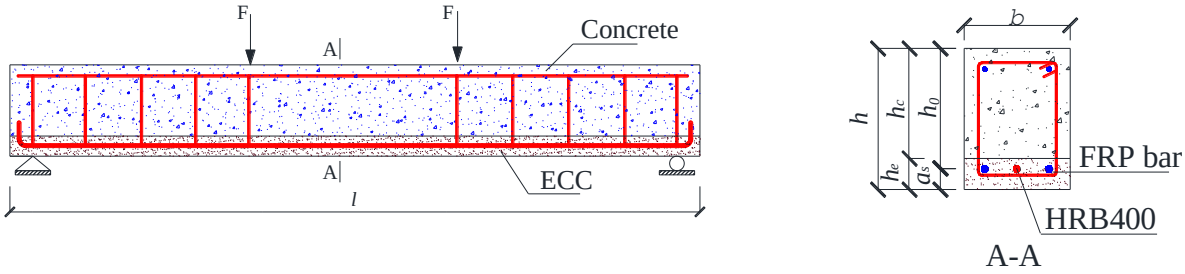

Fig.1. Loading diagram and reinforcement details

Table 1 The cross-section dimensions and material properties for beams

Category	Designation	Details	Unit
Beam	b	Width of beam cross section	mm
	h	Height of beam cross section	mm
	h_0	Effective height of beam cross section	mm
	l	Length of beam	mm
Concrete	f_c	Compressive strength of concrete	MPa
	h_c	Concrete layer height of beam	Mm
ECC	f_{ec}	Compressive strength of ECC	MPa
	f_{et}	Tensile strength of ECC	MPa
	h_e	ECC layer height of beam	mm
	r	ECC height ratio of beam height	--
Reinforcement	f_y	Yield strength of steel bars	MPa
	A_s	Area of tensile reinforcing steel bars	mm^2
	f_{fd}	Design strength of FRP bars	MPa
	A_f	Area of tensile reinforcing FRP bars	mm^2
	ρ	Equivalent ratio of reinforcements	--

The equivalent reinforcement ratio of steel and FRP bars in Table 1, denoted by ρ [24], is

calculated by formula (1). The ECC height ratio of beam height in Table 1, denoted by r, is calculated by formula (2).

$$\rho = \frac{A_s}{bh_0} + \frac{f_{fd}}{f_y} \cdot \frac{A_f}{bh_0} \quad (1)$$

$$r = \frac{h_e}{h} \quad (2)$$

Based on many research papers about machine learning prediction for flexural capacity of concrete beams [25-33], a total of 8 input parameters are selected to develop the prediction model. These parameters are the width of beam cross section (b), effective height of beam cross section (h_0), compressive strength of concrete (f_c), compressive strength of ECC (f_{ec}), tensile strength of ECC (f_{et}), ECC height ratio of beam height (r), yield strength of steel bars (f_y), design strength of FRP bars (f_{fd}), and equivalent ratio of reinforcements (ρ). The statistical information and distribution of input and output features in the established database are shown in Table 2 and Fig. 2, respectively. Kernel density curves were used to demonstrate the trend of data changes as shown in Fig. 2.

In Table 2, when f_c is 0, f_{ec} and f_{et} is non-zero, it indicates that the beam is fully cast from ECC without any concrete layer. Conversely, when f_{ec} and f_{et} are 0, f_c is non-zero, it indicates that the beam is entirely cast from concrete, without an ECC layer. When f_c, f_{ec} and f_{et} are non-zero, it indicates that the beam is an ECC-concrete composite beam. And when f_y is 0 and f_{fd} is non-zero, it indicates that the beam is FRP bars RC beam. When f_{fd} is 0 and f_y is non-zero, it indicates that the beam is steel RC beam. When both f_y and f_{fd} are non-zero, it indicates that the beam is steel and FRP bars hybrid RC beam. V_{min} and V_{max} represent the minimum and maximum values, respectively, Avg represents the average value, σ represents the standard deviation, Cv represents the coefficient of variation. Detailed data are provided in the Appendix.

Table 2 The statistical information of parameters in the database

Feature	Type	V_{min}	V_{max}	Avg	σ	Cv
b (mm)	Input	100	150	139.2	21.3	0.15
h_0 (mm)	Input	116	264	172.3	42.1	0.24
f_c (MPa)	Input	0	80	37.1	19.2	0.51
f_{ec} (MPa)	Input	0	45.2	33.3	15.5	0.46
f_{et} (MPa)	Input	0	4	2.4	1.3	0.54
f_y (MPa)	Input	0	503	321.3	187.7	0.58
f_{fd} (MPa)	Input	0	2437	853	740	0.86
ρ (%)	Input	0.105	9.45	1.4	1.78	1.27

r (%)	Input	0	100	50	35	0.7
M_u (kN·m)	Output	4.42	133.1	29.12	28.48	0.98

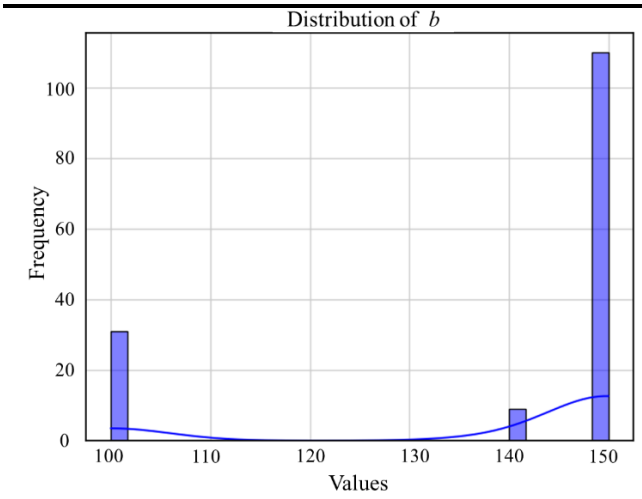

(a) b (mm)

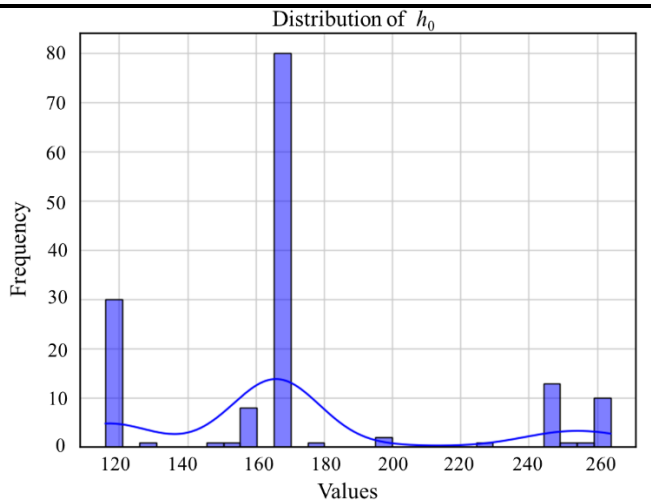

(b) h_0 (mm)

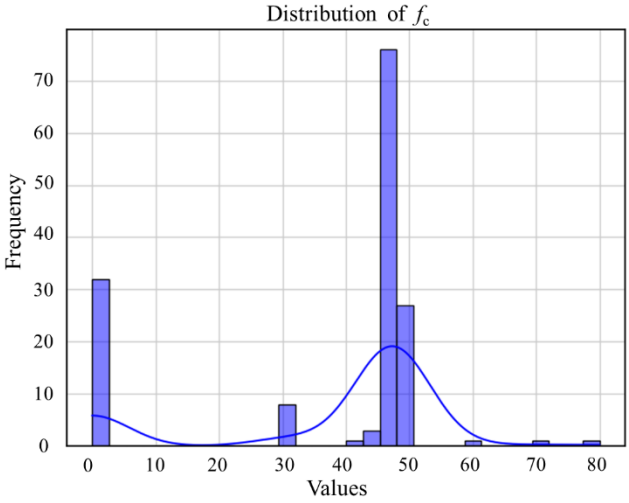

(c) f_c (MPa)

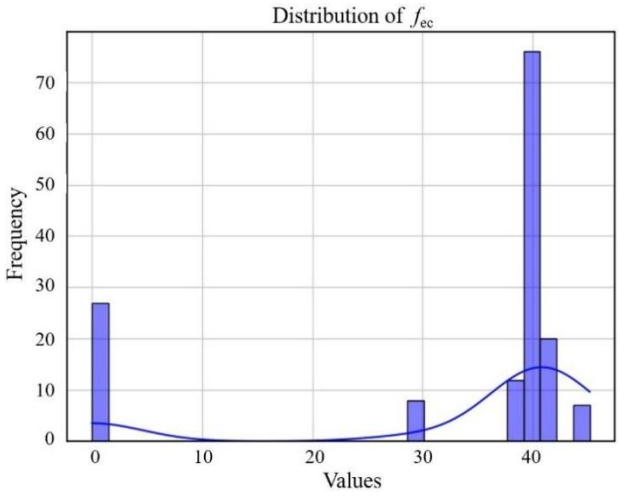

(d) f_{ec} (MPa)

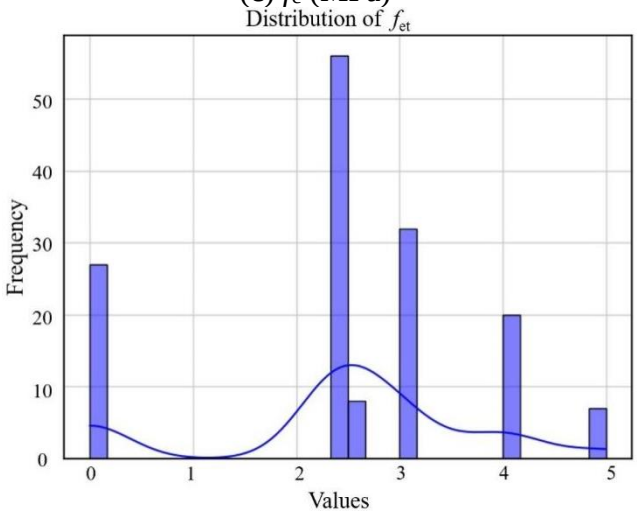

(e) f_{et} (MPa)

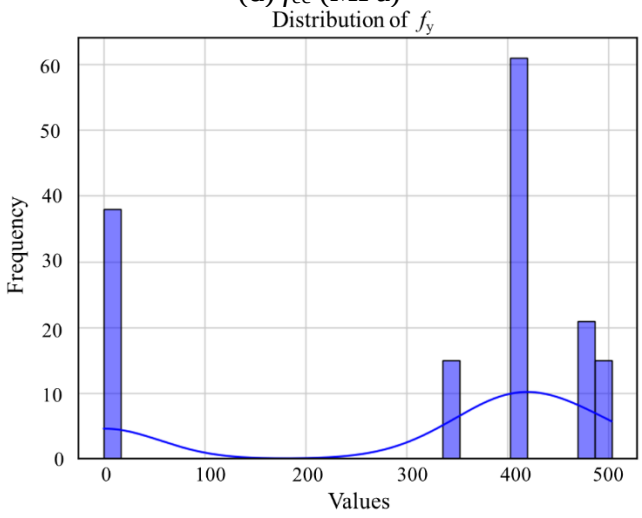

(f) f_y (MPa)

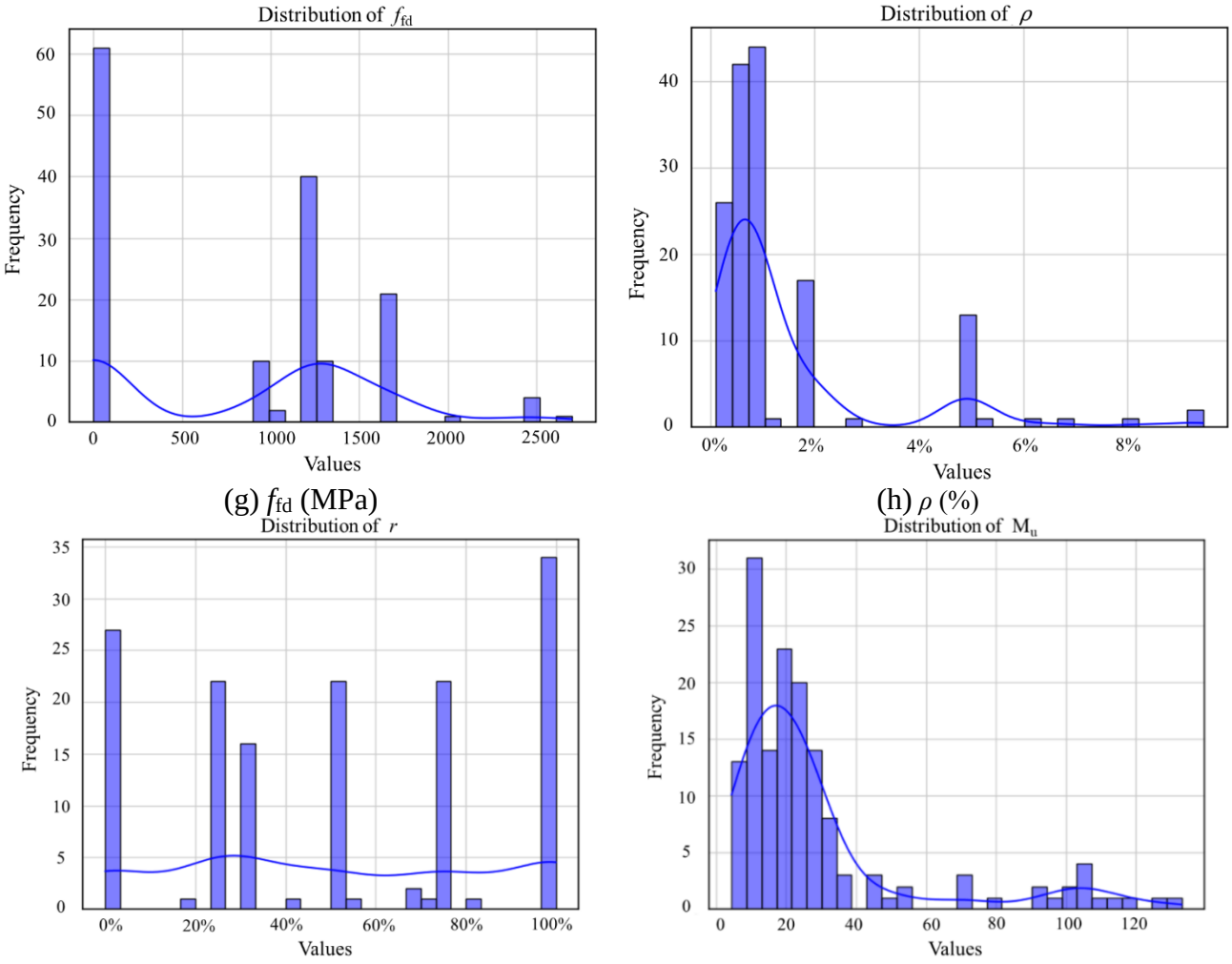

(g) f_{fd} (MPa) (h) ρ (%)

(i) r (%) (j) M_u (kN·m)

Fig.2. Statistical Distribution of Machine Learning Parameters

From Fig.2 , the input parameter b for beam width varies between 100 and 150 mm, while the input parameter h_0 varies between 120 and 260 mm, centered around 160 to 180 mm. The input parameter f_c is distributed between 0 and 80 MPa, the input parameter f_{ec} is distributed between 0 and 45 MPa and the input parameter f_{et} is distributed between 0 and 5 MPa. The input parameter f_y is centered around 350 to 500 MPa, while the input parameter f_{fd} is centered around 900 to 2000 MPa. The input parameter ρ ranges from 0.5% to 7%, with the majority distributed between 0.5% and 2%. The input parameter r is uniformly distributed between 0% and 100%. It can be observed that the input parameters exhibit a wide range of variation, indicating that the machine learning prediction model established based on this database has broad applicability and versatility.

3. Prediction Algorithms and Evaluation Metrics

3.1 Overview of Machine Learning Algorithms

3.1.1 Support Vector Regression

Support Vector Regression (SVR) [34-37] is a supervised learning algorithm model for binary classification. Its basic idea is to find a hyperplane in the feature space that separates samples of different classes, such that the samples of each class are farthest from the hyperplane, thus achieving the optimal solution. It demonstrates excellent performance for both linear and non-linear problems. This paper analyzes the influence of feature parameters such as width of beams, effective height, strength of concrete and ECC, strength of steel and FRP bars, which exhibit a non-linear distribution. In SVR, the original model is transformed into a dual equation, where the objective function involves only the inner product between instances, replaced by a kernel function. The final decision function is represented as Equation (3), where x is the input feature vector, $K(x, x_i)$ is the kernel function replacing the inner product, α_i is the Lagrange multiplier, and a penalty factor C is introduced, where $0 \leqslant \alpha_i \leqslant C$, and b is the distance parameter.

$$f(x) = sign(\sum_{i=1}^{N} \alpha_i y_i K(x, x_i) + b) \tag{3}$$

3.1.2 Extreme Gradient Boosting

Extreme Gradient Boosting (XGBoost) [38-40] is a supervised learning algorithm used for analyzing classification and regression problems. It is an improved version of the Gradient Boosting Decision Tree (GBDT) algorithm, both of which are regression decision tree models. XGBoost introduces parallelization into the boosting process, allowing for faster computation by training on serial data. Additionally, XGBoost introduces second-order partial derivatives of the loss function, resulting in better learning performance. To prevent overfitting, XGBoost adds a regularization term to its objective function, as shown in Equation (4). Here, y_i represents the true output of the i^{th} data point, $\hat{y}_i^{(k-1)}$ denotes the ensemble output of the first $k-1$ learners for the i^{th} data point, $f_k(\cdot)$ is the k^{th} learner being trained, and $\Omega(f)$ is the regularization term introduced.

$$\min_{f_k(x), \Omega(f_j)} (\sum_{i=1}^{n} l(y_i, \hat{y}_i^{(k-1)} + f_k(x_i)) + \sum_{j=1}^{k} \Omega(f_j)) \tag{4}$$

3.1.3 Multilayer Perceptron

Multilayer Perceptron (MLP) [41-43], also known as Artificial Neural Network (ANN), is a three-layer perceptron. Between the layers of the multi-layer perceptron, there are fully connected connections. The lowest layer is the input layer, followed by one or more hidden layers, and the top layer is the output layer. In the working environment of MLP, information is transmitted through the neurons in each layer, and the connection between the hidden layer and the output layer represents a

multi-class logistic regression. All parameters of MLP include the connection weights and configurations between each layer, involving loss functions, regularization terms, and more.

3.1.4 Random Forest

Random Forest (RF) [44-46] is an ensemble learning method capable of effectively handling classification and regression problems. It is also a type of decision tree model. The decision-making process of a decision tree moves from the top node to the leaf nodes. By combining multiple decision trees together, each time selecting the dataset randomly with replacement, and then randomly selecting a subset of features as input, the Random Forest algorithm is formed. In the RF framework model, a regression function is constructed to predict the output value *Y*. This function requires training on input variables similar to decision trees, and then prediction is made using the applicable equation. The regression function is represented as Equation (5), where h_{K} is the K^{th} decision tree, and *x* is the input value.

$$Y = \frac{1}{\mathrm{K}} \sum_{\mathrm{k}=1}^{\mathrm{K}} h_{\mathrm{K}}(x) \tag{5}$$

3.1.5 ExtRa Trees

ExtRa Trees (ERT) is a variant of the Random Forest algorithm [47]. Unlike RF, which uses random sampling with replacement (bootstrap) to select sampling datasets for training each decision tree, ERT does not use random sampling. Instead, each decision tree in ERT utilizes the original training dataset. After selecting the input features for partitioning, the decision trees in RF choose the optimal feature values for partitioning based on criteria such as coefficients and variances. However, ERT randomly selects a feature value for partitioning decision trees. Therefore, sometimes ERT exhibits better generalization performance than RF.

3.2 Evaluation Metrics

In statistical measurement methods, to evaluate the effectiveness of a machine learning algorithm, commonly used metrics include Root Mean Square Error (RMSE), Mean Absolute Error (MAE), Coefficient of Determination (R^2), and Mean Absolute Percentage Error (MAPE). These evaluation metrics objectively assess the degree of proximity between the model's predictions and the actual values. In a well-performing model, lower values of RMSE, MAE, and MAPE indicate better performance, while R^2 values closer to 1.00 indicate better fit [48]. The evaluation formulas are shown as Equation (6)~(9). Where y、$\hat{y}$、$\overline{y}$, and *n* represent the actual values, predicted values, mean value, and number of data points, respectively.

$$RMSE = \sqrt{\frac{1}{n}\sum_{i=1}^{n}(\hat{y} - y_i)^2} \quad (6)$$

$$MAE = \frac{1}{n}\sum_{i=1}^{n}|\hat{y} - y_i| \quad (7)$$

$$R^2 = 1 - \frac{\sum_{i=1}^{n}(\hat{y} - y_i)^2}{\sum_{i=1}^{n}(\overline{y} - y_i)} \quad (8)$$

$$MAPE = \sum_{i=1}^{n}\frac{1}{n}\left|\frac{y_i - \hat{y}}{y_i}\right| \quad (9)$$

4. Model development and discussion

This section presents the development process of interpretable machine learning models (SVR, XGBoost, MLP, RF, and ERT) and discusses the related model performance. The overall structure of the developed models is illustrated in Fig. 3. The methodology for constructing the prediction models includes database establishment, data preprocessing, model training, optimal hyperparameter tuning, model validation, and model interpretation.

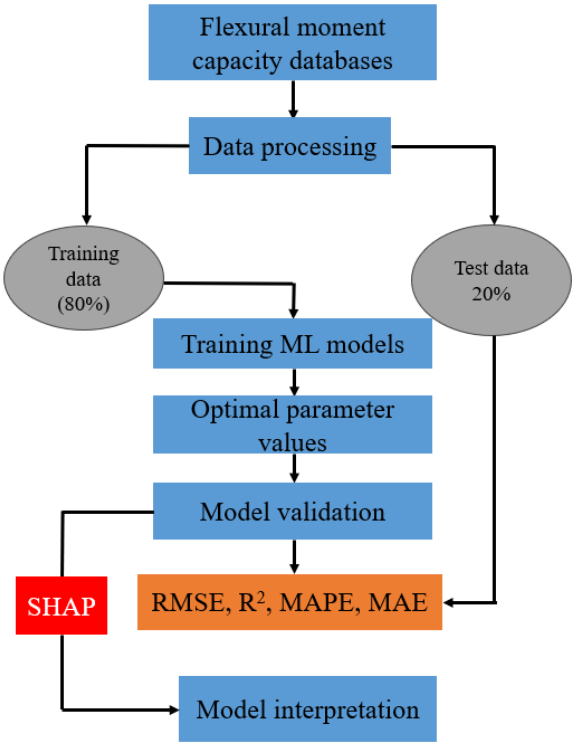

Fig.3 Overall structure of the developed ML models

Firstly, experimental research data on the flexural capacity of ECC-concrete composite beams hybrid reinforced with steel and FRP bars were extracted from the literature and compiled into a database table. Eight parameters were selected as input features, while the flexural capacity served as the output feature. This database was used to train machine learning models, and all machine

learning algorithm models were built using the sklearn module in Python. The 150 experimental data points in the database were divided, with 80% of the data used for training the machine learning algorithm models and the remaining 20% used as a test dataset to evaluate the performance of each algorithm's model. The performance of each model algorithm's predictive ability was evaluated using RMSE, MAE, R^2, and MAPE. Finally, for the best-performing model, the Shapely weighted explanation (SHAP) value analysis method was employed to visualize and interpret the predictive model, providing a better understanding of the importance of the relationship between bending capacity and input variables.

4.1 Optimization of the model parameters

To optimize the performance of each machine learning algorithm, a 6-fold cross-validation grid search technique was employed to optimize the parameters of the five machine learning algorithms. The grid search technique performs CV iterations for each parameter combination in the parameter grid list and selects the combination with the highest average score as the optimal choice. The GridSearchCV function in the sklearn module was utilized to perform 6-fold cross-validation grid search learning and extracted the optimal combination values of the parameters. The main parameter selections for the five machine learning algorithms are shown in Table 3. Other parameters of the models are set by default using the sklearn module. The parameter selections for each model are presented in Table 3.

Table 3. Optimal parameter values for ML models

ML Models	Parameters	Values	Best values
SVR	kernel	linear, poly, rbf, sigmoid	rbf
	C	1000, 2000, 3000	2000
	gamma	0.1, 0.2, 0.3	0.2
XGBoost	learning_rate	0.03, 0.3, 3	0.03
	n_estimators	300, 400, 500, 600	400
	max_depth	2, 3, 4	3
MLP	activation	logistic, tanh, relu	relu
	max_iter	6000, 8000, 10000	8000
	learning_rate	0.001, 0.01, 0.1	0.01
RF	n_estimators	800, 1000, 1200	1000
	max_depth	5, 10, 15	10
ERT	n_estimators	800, 1000, 1200	1000
	max_depth	5, 10, 15	10

4.2 Analysis of ML model performance

Once the optimal parameters for each machine learning algorithm are determined, these parameters are input into each algorithm. Utilizing the training dataset from the database, five different machine learning models are constructed. The performance of these models is evaluated by comparing the predicted results with the experimental values. The comparison between the results obtained from the SVR, XGBoost, MLP, RF, and ERT machine learning models and the experimental moment capacity is illustrated in Fig. 4.

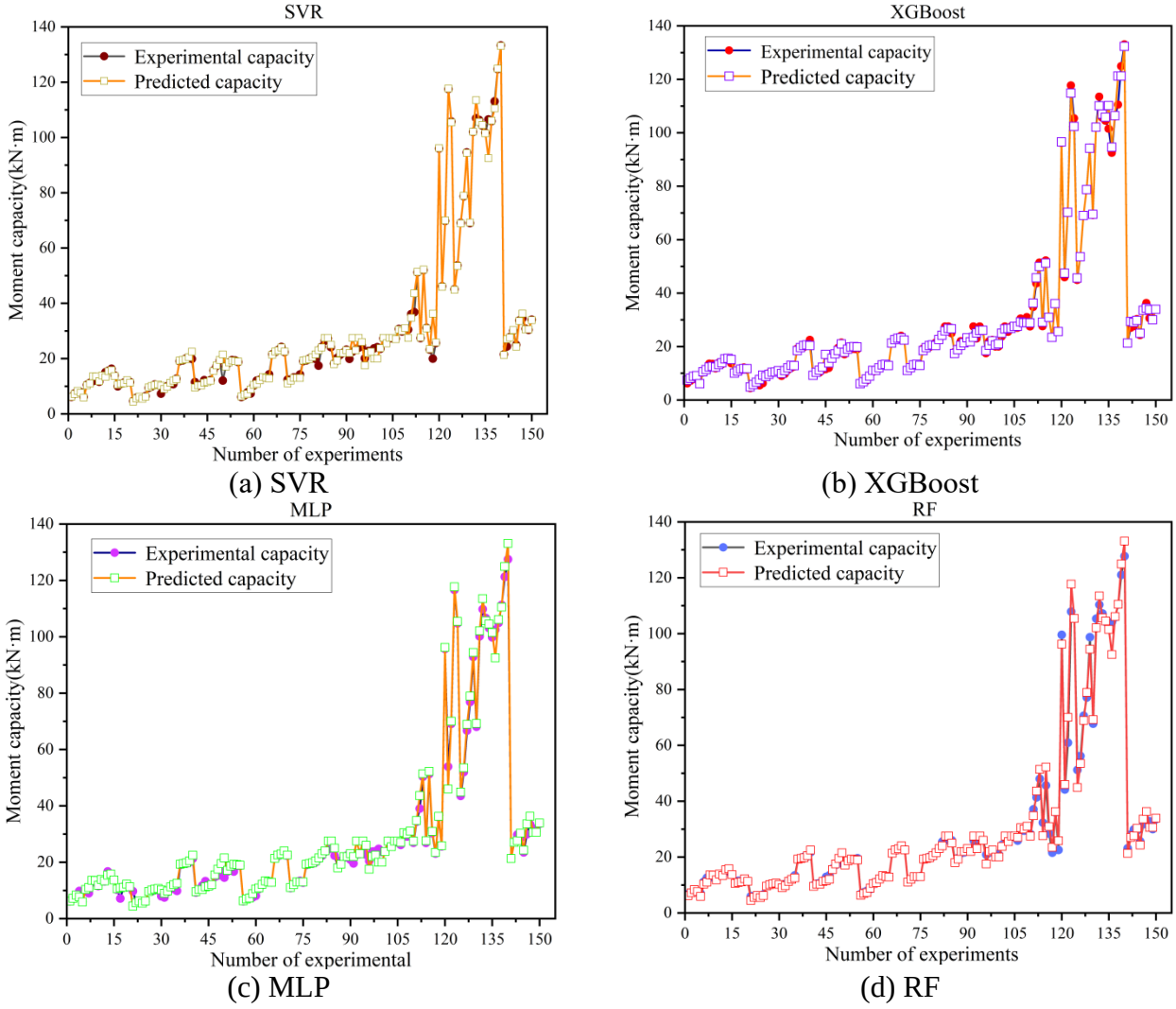

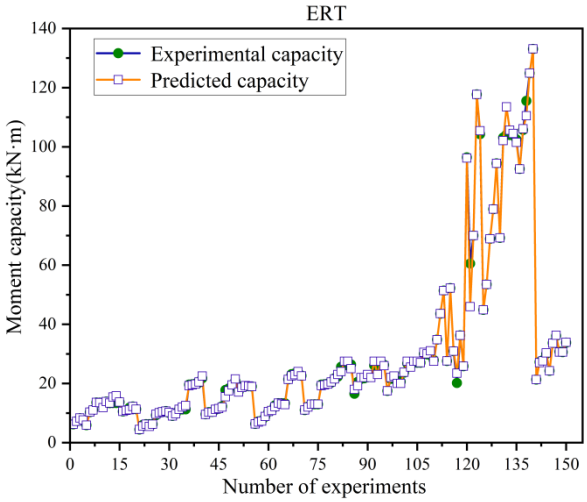

(e) ERT

Fig.4. Comparison of experimental and predicted values of ML models

Fig.4 shows that all the five machine learning algorithms demonstrate good predictive capabilities for the bending capacity of steel and FRP bars hybrid reinforced ECC-concrete composite beams. Among them, the conformity of XGBoost, MLP, and ERT algorithm models is significantly higher than those of the other two algorithms. Furthermore, to accurately assess the predictive performance of each algorithm and better understand the comparison between predicted and experimental values, linear fitting plots of the predicted and experimental moment capacities for the five algorithm models are shown in Fig.5. In this figure, the experimental values are plotted on the x-axis, and the predicted values are plotted on the y-axis. The diagonal line (y=x) indicates equivalence between predicted and experimental values, with more points accumulating along this line suggesting more accurate model predictions. Additionally, the training and testing datasets were marked on the plot to provide clearer insight into the response of both datasets. Moreover, dashed lines representing -10% (y=0.9x) and +10% (y=1.1x) error ranges are plotted above and below the diagonal line (y=x), considering data points within this error range as reasonably accurate.

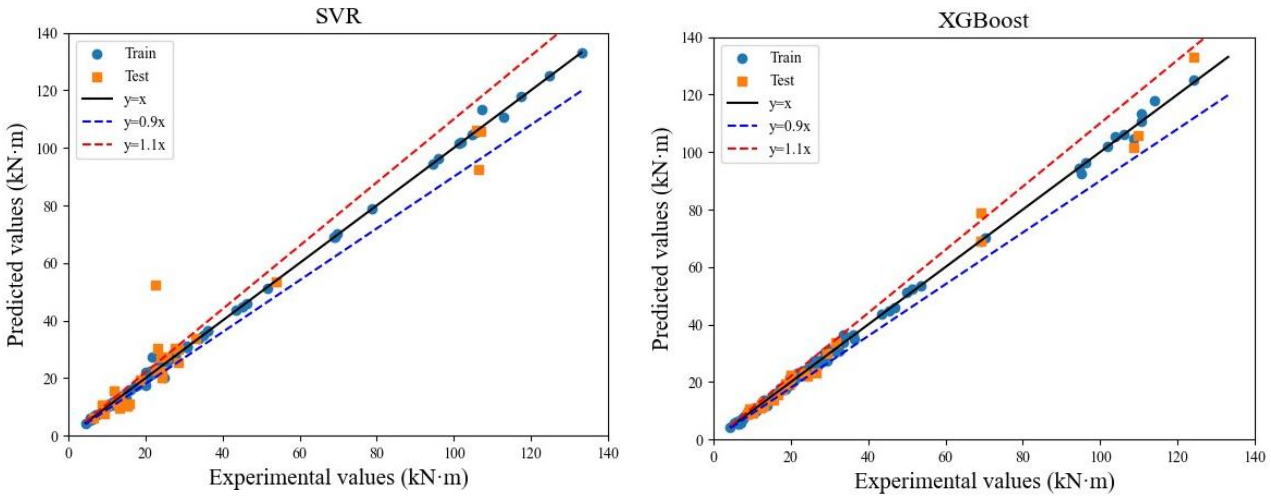

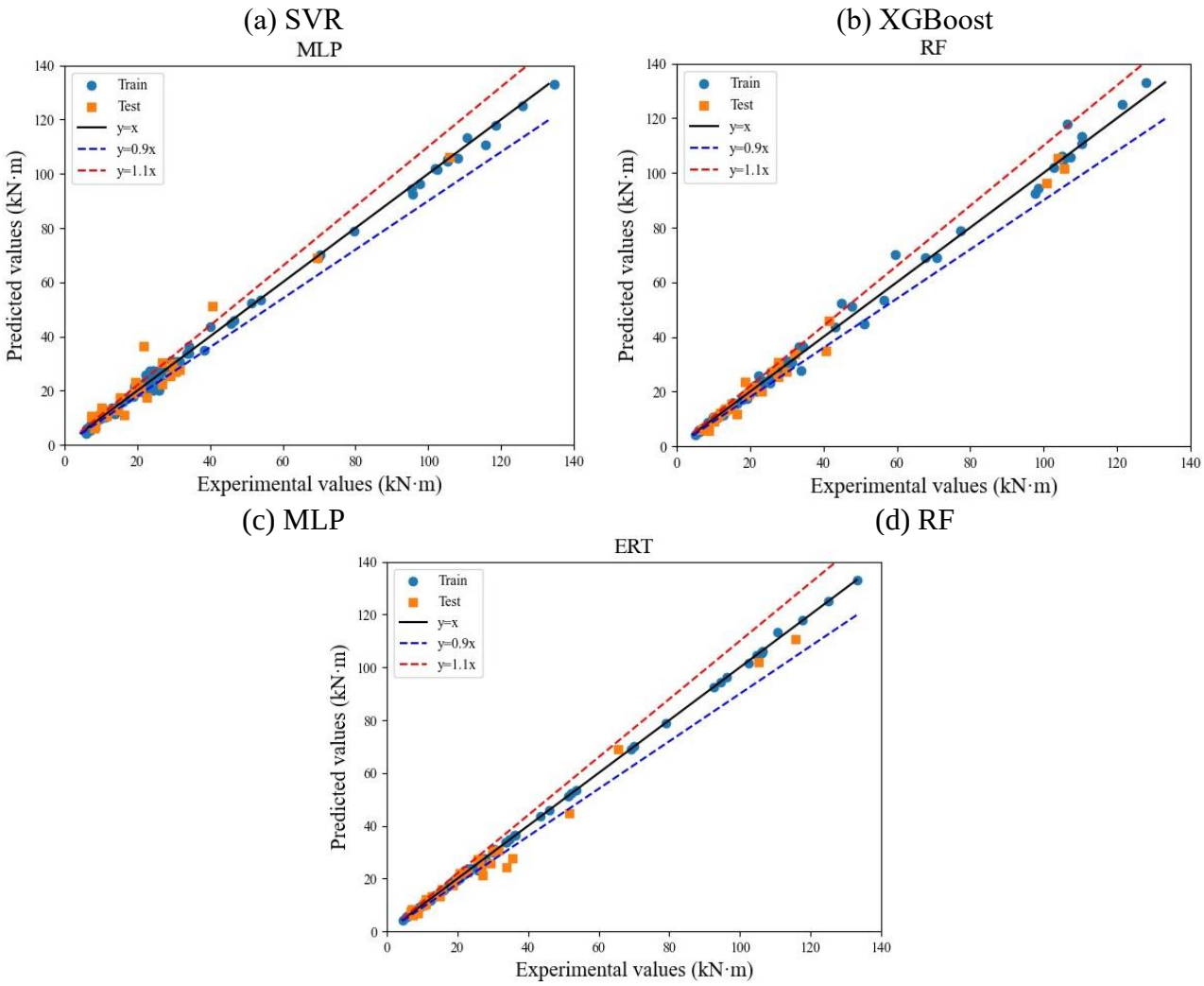

Fig.5 The linear fitting plot between the experimental capacity and the predicted capacity of ML models

From Fig.5, it is evident that the five different ML algorithm models exhibit their learning and predictive capabilities on both training and testing values. Among them, the performance of XGBoost model is significantly better than other models. The MLP and ERT models show instances where data points lie outside the permissible error range. Therefore, XGBoost demonstrates superior performance in predicting the moment capacity of steel and FRP hybrid reinforced ECC-concrete composite beams.

Additionally, the performance metrics, including RMSE, MAE, MAPE, and MAE, for the training and testing datasets under the five models was summarized, as shown in Table 4. Furthermore, the radar charts for the performance indicators of the training and testing datasets for each model were plotted as shown in Fig.6, aiming to compare the machine learning models used in this study.

Table 4 Performance metrics of ML model

ML model	Dataset	RMSE	MAE	R^2	MAPE
SVR	Training	1.463	0.612	0.965	0.031
	Test	5.541	2.923	0.956	0.166
XGBoost	Training	1.402	1.082	0.984	0.046
	Test	2.481	1.536	0.965	0.071
MLP	Training	1.697	0.834	0.978	0.030
	Test	4.792	3.205	0.934	0.239
RF	Training	2.253	1.116	0.944	0.169
	Test	4.654	2.849	0.925	0.215
ERT	Training	1.196	1.299	0.973	0.027
	Test	3.901	2.675	0.958	0.103

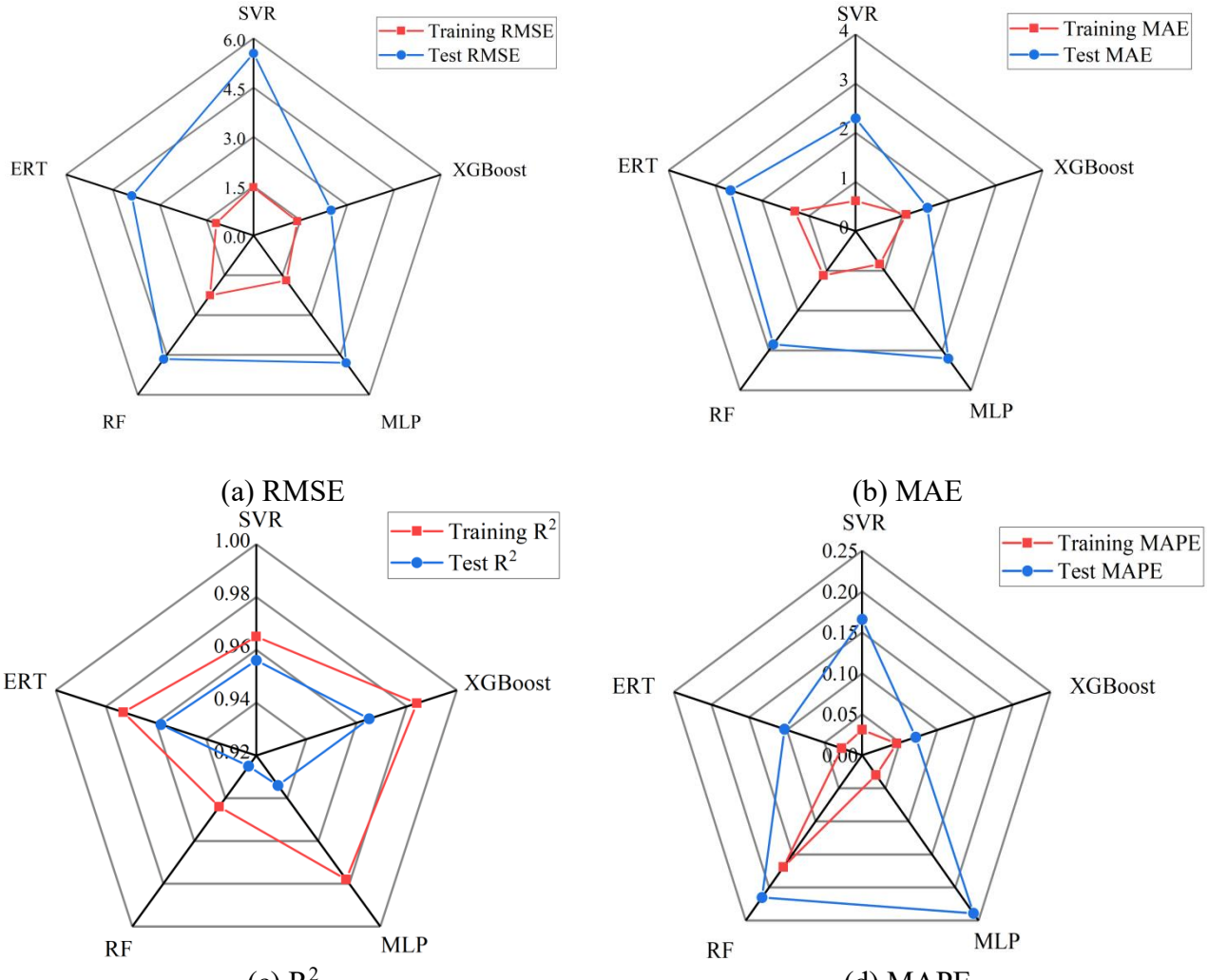

(a) RMSE (b) MAE

(c) R^2 (d) MAPE

Fig.6 Radar chart of performance metrics for machine learning models

From Table 4 and Fig.6, it can be observed that all developed ML models have achieved a high level of learning and prediction capability. There are minor differences among the models, which can be attributed to the different learning methods and limitations of each model. The data shows

that the ERT model exhibits excellent learning and training performance, with the lowest values of RMSE=1.196 and MAPE=0.027 among the five machine learning models on the training dataset. However, the XGBoost model shows comparable performance to the ERT model in terms of learning and training, with the highest R^2=0.984 among the five models on the training dataset. Moreover, the XGBoost model outperforms other models significantly in terms of prediction performance, with the lowest values of RMSE=2.481, MAE=1.536, and MAPE=0.071 on the testing dataset, as well as the highest R^2=0.965 on the testing dataset among all models. Therefore, the evaluation metrics indicate that all developed machine learning models can accurately predict the moment capacity of ECC-concrete composite beams reinforced with steel and FRP bars. Although the ERT model demonstrates good learning and training performance, the XGBoost model exhibits better balance and prediction accuracy.

To better assess the performance of each model, Taylor diagrams were plotted to evaluate the learning, training, and prediction capabilities of each model. Taylor diagrams essentially integrate three evaluation metrics of the model: correlation coefficient, center root-mean-square error, and standard deviation, onto a single coordinate graph, based on the cosine relationship among them [25]. By comparing the distances between the model-simulated and the tested data points, the model that is closest to the experimental data points demonstrates the best simulation performance. Currently, Taylor diagrams have been widely used to assess the performance of fiber reinforced composite materials. Fig.7 depicts the Taylor diagrams of the five machine learning models for the moment capacity of ECC-composite beams hybrid reinforced with steel and FRP bars in the training and testing datasets. In the figure, the purple dashed line represents the scale of the center root-mean-square error, the radial axes represent the normalized standard deviation, and the circular arcs represent the correlation coefficients. From both plots, it can be observed that XGBoost exhibits higher correlation coefficients and lower standard deviation and center root-mean-square error in both learning and prediction phases. Its model data points are closer to the true data points, demonstrating the best learning and training performance, and its prediction performance is closest to the experimental data.

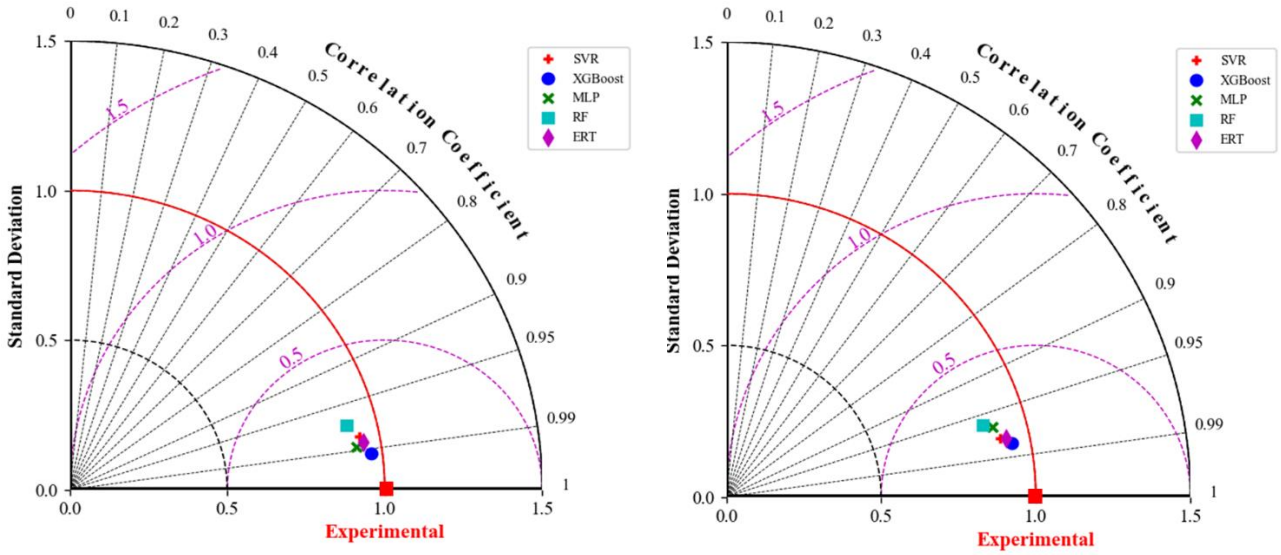

(a) Training dataset (b) Test dataset

Fig.7 Taylor diagram presentation of ML models

5. Assessment of Input Parameter Variable Importance and Correlation

In recent years, given the impact of machine learning models on scientific research, efforts have been made to develop a method capable of explaining these models, namely Shapley Additive Explanations (SHAP) [49]. SHAP additive explanations are popular in machine learning models as they help individuals understand the importance of each input variable on the output variable [50]. This explanatory method can address the issue of multicollinearity by not only considering the influence of individual variables but also taking into account the impact of variable groups and potential synergistic effects between variables. It calculates the average marginal effect of each input parameter by evaluating the magnitude of feature variable attributes, including all possible combinations. The absolute value of the resulting SHAP values is used to determine the contribution of each input parameter to the output parameter; the higher the SHAP value, the greater the impact of the input parameter on the output parameter [51]. Therefore, in this study, SHAP additive explanations were applied to the XGBoost model with the best predictive performance, as shown in Fig.8.

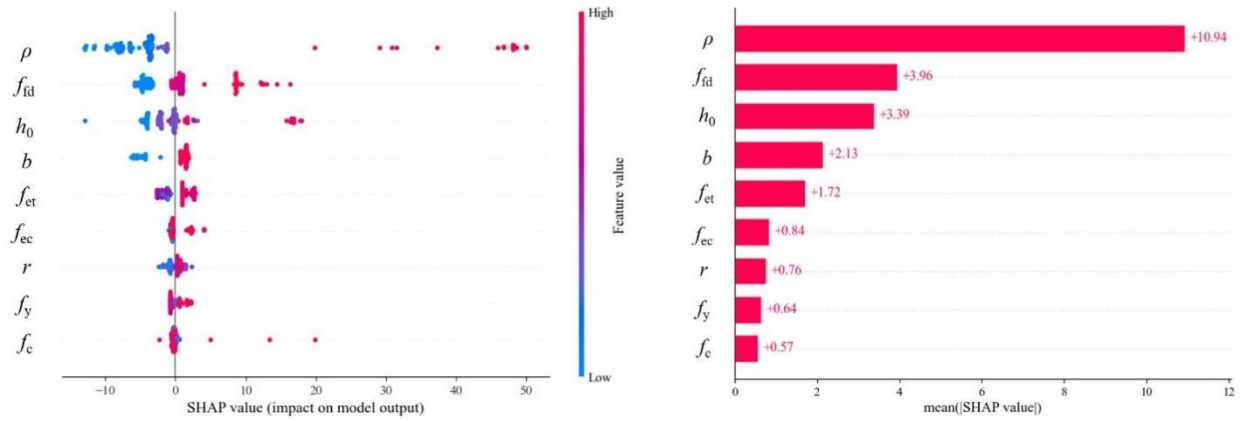

(a) SHAP value (b) mean |SHAP value|

Fig.8 SHAP summary plot for input features

In Fig. 8 (a), each data sample is represented by a point, where the horizontal position of these points indicates the SHAP value calculated for the given input feature. Positive SHAP values indicate increasing influence of the input feature on the model output, while negative SHAP values represent decreasing influence of the input variable. Additionally, coloring is applied to the input feature values within each data sample, with blue shading for low values, red shading for high values, and purple shading near the mean to provide visualization. Moreover, the width of the color region for each feature variable indicates the magnitude of its influence. In Fig.8 (b), passing the SHAP value matrix to the bar plot function will create a global feature importance plot, where the global importance of each feature is considered as the average absolute value of that feature across all given samples. The *x*-axis represents the mean absolute SHAP value, while the *y*-axis sorts the input variables based on their importance, with the input variable having the highest contribution positioned at the top. As shown in Fig. 8, when examining the factors affecting the bending capacity of steel and FRP bars hybrid reinforced ECC-concrete composite beams, it is found that the equivalent reinforcement ratio (ρ), design strength of FRP bars (f_{fd}) and effective beam depth (h_0) have significantly influence. However, from the SHAP analysis plot, it is less obvious that the compressive strength of concrete (f_c) has a significant impact on the bending capacity.

From reviewing the literature and relevant documents, there are three methods to measure the correlation density between variables: the Pearson correlation coefficient, the Spearman rank correlation coefficient, and the Kendall rank correlation coefficient. The Pearson correlation coefficient is used for continuous variables and requires the assumption of a normal distribution. The Kendall rank correlation coefficient is suitable for ordered categorical variables. The Spearman rank correlation coefficient has a broader scope of application and fewer prerequisites. It is used for ordinal variables and interval data that do not meet the assumption of a normal distribution. The specific formulas are shown below.

Fig. 9 presents the Spearman rank correlation matrix for input features. It can be observed from the figure that among the beam dimension parameters, there is a notable correlation between beam width and effective height. Despite this correlation, these two parameters were independent variables as reported in the data collected. In the ECC-related parameters, a significant correlation is evident between f_{ec} and f_{et}, as anticipated. Additionally, r shows correlation with both f_{ec} and f_{et}, though the correlation is not significant.

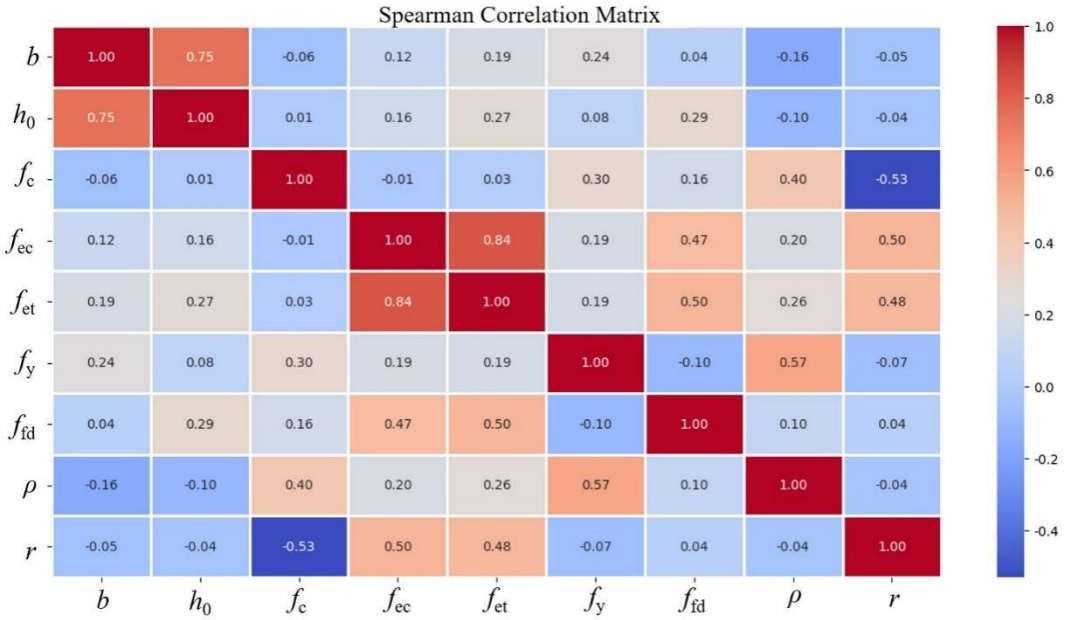

Fig.9 Spearman Correlation Matrix for input features

Passing the SHAP value matrix to a heatmap for visualization, where instances are on the x-axis and model outputs are on the y-axis, SHAP values are encoded according to a color scale. The samples are sorted based on hierarchical clustering according to explanatory similarity, grouping samples with similar reasons for model output together. The SHAP heatmap is depicted in Fig.10, with the model's outputs displayed above the heatmap matrix, and the global importance of each input parameter shown as a bar plot on the right-hand side in black. The $f(x)$ value above the image represents the model's output, with the gray dashed line indicating the baseline. The $f(x)$ curve demonstrates different SHAP values detected for similar $f(x)$ values. From Fig.10, it's evident that the most effective input feature for the bending capacity of steel and FRP bars hybrid reinforced ECC-concrete composite beams is the equivalent reinforcement ratio (ρ), while the least effective input feature is the compressive strength of concrete (f_c). By exporting the SHAP additive explanation plots and SHAP heatmap obtained from the XGBoost model, our understanding about how input features affect the bending capacity of steel and FRP bars hybrid reinforced ECC-concrete composite beams is greatly enhanced.

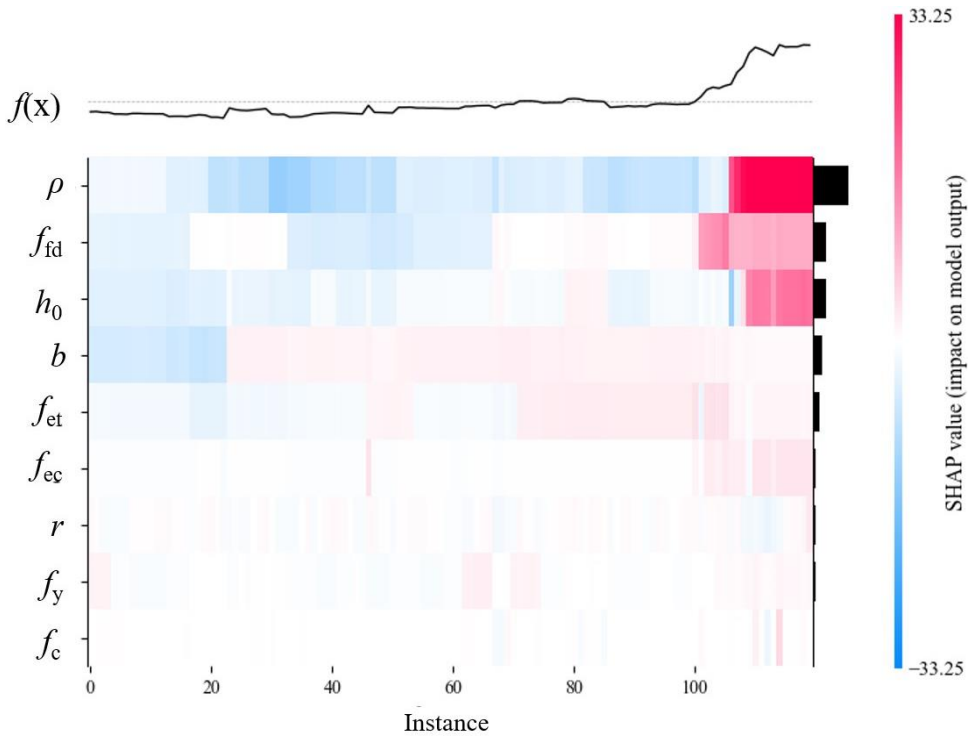

Fig.10 SHAP heat maps for input features

6. Graphical user interface development

In the development of machine learning models, it is particularly important to create a user interface application that allows direct interaction by researchers and engineers, aiming to popularize the widespread use of these models in engineering applications. A Graphical User Interface (GUI) facilitates users' understanding of complex data analysis and model outcomes, enabling them to better comprehend and optimize the behavior of the model by adjusting parameters and input values. This interface opens up the use of machine learning models to a wider audience, making the complex analysis process more understandable and facilitating communication between developers and users to improve the reliability of model results [52]. The GUI application is developed based on the tkinter module in the Python programming language, where developers can utilize simple components such as text boxes, buttons, and labels to implement GUI development.

Therefore, this paper developed a GUI application based on the XGBoost model, which, as demonstrated in the comparison of five machine learning models in the previous section, exhibits higher accuracy. As shown in Fig.11, the GUI application developed can easily allow the users to input their own calculated data to predict the moment capacity of ECC-concrete composite beams hybrid reinforced with steel and FRP bars. For example, when the width of the beam cross-section is 150 mm, the yield strength of steel bar is 340 MPa, the effective height of beam is 166 mm, the

design strength of FRP bar is 1260 MPa, the compressive strength of concrete is 47 MPa, the compressive strength of ECC is 41 MPa, the equivalent reinforcement ratio is 0.5%, the tensile strength of ECC is 3 MPa, and the ECC height ratio of beam height is 50%, the output flexural moment capacity is 26.97 kN·m. By creating a GUI module in the Python programming language, such development contributes to solving complex problems and expanding interfaces for interaction with humans.

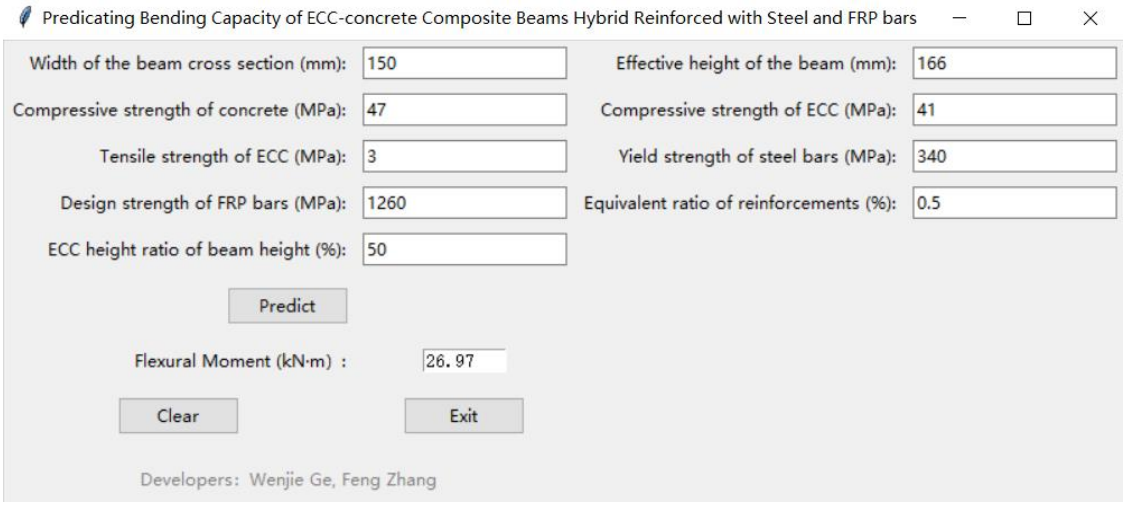

Fig.11 GUI for predicting bending capacity of ECC-concrete composite beams hybrid reinforced with steel and FRP bars

7. Conclusion

This study comprehensively investigates the bending capacity of steel and FRP bars hybrid reinforced ECC-concrete composite beams by using five different machine learning algorithm models (SVR, XGBoost, MLP, RF, and ERT). Utilizing 150 datasets from literature, analysis and organization of eight feature parameters were conducted, leading to the development of the most accurate model. Furthermore, employing the SHAP method, the impact of each input parameter on the bending capacity of steel and FRP bars hybrid reinforced ECC-concrete composite beams was evaluated, obtaining the following conclusions.

1) All five machine learning algorithm models used in the study demonstrate good predictive performance. Among them, ERT exhibits superior training performance, with the lowest values of RMSE=1.196 and MAPE=0.027 among all models on the training dataset. However, XGBoost achieves the best predictive performance, with the lowest values of RMSE=2.481, MAE=1.536, and MAPE=0.071 among all models on the testing dataset. Additionally, XGBoost attains the highest R^2 value of 0.965 on the testing dataset, surpassing all other models.

2) From the radar chart depicting the performance of the five machine learning algorithm models, it is evident that XGBoost exhibits superior balance and predictive accuracy. Analysis via Taylor diagrams reveals that, both in training and prediction scenarios, the data points of the XGBoost model are closest to the actual values, illustrating its optimal learning performance. Moreover, the predicted values are closest to the actual experimental values.

3) According to the Spearman correlation matrix plot of the 150 experimental data points collected, a significant correlation exists between width and effective height within beam dimension parameters. Among ECC input parameters, there is a clear correlation between compressive and tensile strength. Additionally, there is a weak correlation between ECC height ratio of beam height and compressive/tensile strength.

4) According to the analysis results of the SHAP additive explanation plot and the SHAP heat map, the equivalent reinforcement ratio (ρ), design strength of FRP bars (f_{fd}) and effective height of the beam (h_0) have significant impacts on the bending capacity. These are important input parameters. In comparison with other features, the influence of the compressive strength of concrete (f_c) on flexural capacity is less pronounced.

5) A graphical user interface (GUI) application was developed to accurately predict the bending capacity of steel and FRP bars hybrid reinforced ECC-concrete composite beams. The GUI can assist design engineers and researchers in estimating the bending capacity while significantly reducing the need for expensive test materials and complex experimental testing.

This study provides a theoretical basis for predicting the bending capacity of ECC-concrete composite beams hybrid reinforced with steel and FRP bars. As the results of this study are limited to the selected parameters, future work will focus on developing prediction expressions applicable to a wider range of variable parameters using machine learning methods with more extensive parameter data.

Acknowledgments

The authors would like to acknowledge financial support from the High-End Foreign Experts Project of Ministry of Science and Technology, China (G2022014054L), the Science and Technology Project of Jiangsu Construction System (2023ZD104 and 2023ZD105), the Science and Technology Cooperation Fund Project of Yangzhou City and Yangzhou University (YZ2022194), the Yangzhou Construction System Science and Technology Project (202309 and 202312), the Nantong Jianghai (226) talents project and the Research Project of Jiangsu Civil Engineering and

Architecture Society (the Second Half of 2022).

References

[1] Zhiqiang Dong, Gang Wu, Xaioling Zhao, Hong Zhu, Xinxing Shao. Behaviors of hybrid beams composed of seawater sea-sand concrete (SWSSC) and a prefabricated UHPC shell reinforced with FRP bars[J].Construction and Building Materials, 2019(213) 32-42.

[2] Liu Jin, Xinyu Zhao, Renbo Zhang, Xiuli Du. Evaluation of impact response of thermal-damaged FRP-RC slabs: Effects of FRP bar type and concrete cover thickness[J]. Journal of Building Engineering, 2023 (75).

[3] Victor C. Li, Tetsushi Kanda. Innovations Forum: Engineered Cementitious Composites for Structural Applications[J]. Journal of Materials in Civil Engineering, 1998, 19(7): 66-69.

[4] Victor C. Li, Christopher K.Y. Leung. Steady-rate and Multiple Cracking of short Random Fiber Composites[J]. Journal of Materials in Civil Engineering, 1992, 8(11): 2246-2264.

[5] Hayder Alaa Hasan, M. Neaz Sheikh, Muhammad N.S. Hadi. Maximum axial load carrying capacity of Fibre Reinforced-Polymer (FRP) bar reinforced concrete columns under axial compression[J]. Structures, 2019(19): 227-233.

[6] Lieping Ye, Peng Feng. Applications and development of fiber-reinforced polymer in engineering structures[J]. China Civil Engineering Journal, 2006(03): 24-36. (In Chinese)

[7] Xinyu Shen, Bo Li, Weizhuo Shi, Yung-Tsang Chen. Numerical study on flexural behaviour of FRP reinforced concrete beams with compression yielding blocks[J]. Case Studies in Construction Materials, 2022 (17).

[8] Mohammad Z. Afifi, Hamdy M. Mohamed, Brahim Benmokrane. Theoretical stress–strain model for circular concrete columns confined by GFRP spirals and hoops[J]. Engineering Structures, 2015 (102): 202-213.

[9] Lei Pang, Wenjun Qu, Peng Zhu, Jiajing Xu. Design Propositions for Hybrid FRP-Steel Reinforced Concrete Beams[J]. Journal of Composites for Construction, 2016, 20(4).

[10] Mohamed Saafi, Houssam Toutanji. Flexural Capacity of Prestressed Concrete Beams Reinforced with Aramid Fiber Reinforced Polymer (AFRP) Rectangular tendons[J]. Construction and Building Material, 1998, 12(5): 245-249.

[11] Mohammad Mohtasham Moein, Ashkan Saradar, Komeil Rahmati, Seyed Hosein Ghasemzadeh Mousavinejad, James Bristow, Vartenie Aramali, Moses Karakouzian. Predictive models for concrete properties using machine learning and deep learning approaches: A

review[J]. Journal of Building Engineering,2023 (63).

[12] C. Kina, K. Turk, E. Atalay, I. Donmez, H. Tanyildizi. Comparison of extreme learning machine and deep learning model in the estimation of the fresh properties of hybrid fiber reinforced SCC[J].Neural Computing and Applications, 2021 (33).

[13] Tuken Ahmet, Abbas Yassir M., Siddiqui Nadeem A. Efficient prediction of the load-carrying capacity of ECC-strengthened RC beams-An extra-gradient boosting machine learning method[J]. Structures, 2023 (56).

[14] Tadesse G. Wakjira, Abathar Al-Hamrani, Usama Ebead, Wael Alnahhal,. Shear capacity prediction of FRP-RC beams using single and ensenble ExPlainable Machine learning models[J]. Composite Structures, 2022 (287).

[15] Zhihua Xiong, Jiawen Li, Zhu Houda, Xuyao Liu, Zhuoxi Liang. Ultimate Bending Strength Evaluation of MVFT Composite Girder by using Finite Element Method and Machine Learning Regressors [J]. Latin American Journal of Solids and Structures, 2022, 19(3)

[16] Tan Chen. Study on flexural performance of reinforced concrete composite beam reinforced ECC Under freezing and thawing cycles[D].Yangzhou University, 2017.(In Chinese)

[17] Xiao Feng. Study on the Flexural Behavior of ECC-concrete Composite Beams Reinforced with FRP Bar after Freeze-thaw Cycle[D].Yangzhou University, 2018.(In Chinese)

[18] Biyuan Wang. Study on ECC Mechanical Properties and Flexural Performance of Concrete Composite Beams Reinforced with Steel Bars or FRP Bars[D].Yangzhou University, 2016.(In Chinese)

[19] Linglong Pan. Study on the flexural behavior of ECC-concrete composite beam reinforced with steel bars[D]. Yangzhou University, 2018.(In Chinese)

[20] Junyu Chen. Study on the flexural behavior of ECC-concrete composite beams hybrid reinforced steel bar and FRP bar[D].Yangzhou University, 2018.(In Chinese)

[21] Zufa Jiang. Study on Flexural Behavior of FRP Rebar Reinforced ECC Beams[D].Zhengzhou University, 2021. (In Chinese)

[22] Ren Hu. Experimental Study on the Flexural Behavior of ECC-Concrete Composite Beams Hybrid Reinforced with Steel and FRP bars[D]. East China Jiaotong University, 2021. (In Chinese)

[23] Shuo Wang. Research on flexural performance of GFRP-ECC composite beam[D]. Hubei University of Technology, 2020. (In Chinese)

[24] Wenjie Ge; Ashraf F. Ashour; Jiamin Yu, Peiqi Cao, Dafu Cao, Cai Chen, Xiang Ji. Flexural Behavior of ECC-Concrete Hybrid Composite Beams Reinforced with FRP and Steel Bars[J].Journal of Composites for Construction, 2019, 23(1).

[25] M.K. Almustafa, M.L. Nehdi. Machine learning model for predicting structural response of RC slabs exposed to blast loading[J]. Engineering Structures, 2020 (221).

[26] Cailong Ma, Sixuan Wang, Jianping Zhao, Xufeng Xiao, Chenxi Xie, Xinlong Feng. Prediction of shear strength of RC deep beams based on interpretable machine learning[J]. Construction and Building Materials, 2023 (387).

[27] Dade Lai, Cristoforo Demartino, Yan Xiao. Interpretable machine-learning models for maximum displacements of RC beams under impact loading predictions[J].Engineering Structures, 2023 (281).

[28] S. Lee, C. Lee. Prediction of shear strength of FRP-reinforced concrete flexural members without stirrups using artificial neural networks[J].Engineering Structures, 2014 (61).

[29] Tianyu Hu, Hong Zhang, Jianting Zhou. Machine learning-based model for recognizing the failure modes of FRP-strengthened RC beams in flexure[J]. Case Studies in Construction Materials, 2023 (18).

[30] Tadesse G. Wakjira, Mohamed Ibrahim, Usama Ebead, M. Shahria Alam. Explainable machine learning model and reliability analysis for flexural capacity prediction of RC beams strengthened in flexure with FRCM[J]. Engineering Structures, 2022 (255).

[31] Tadesse Gemeda Wakjira, Usama Ebead, M. Shahria Alam, Machine learning-based shear capacity prediction and reliability analysis of shear-critical RC beams strengthened with inorganic composites[J]. Case Studies in Construction Materials, 2022 (16).

[32] Fangming Deng, Yigang He, Shuangxi Zhou, Yun Yu, Haigen Cheng, Xiang Wu. Compressive strength prediction of recycled concrete based on deep learning[J]. Construction and Building Materials,2018 (175).

[33] Feng Zhang, Chenxin Wang, Jun Liu, Xingxing Zou, Lesley H. Sneed, Yi Bao, Libin Wang. Prediction of FRP-concrete interfacial bond strength based on machine learning[J].

Engineering Structures, 2023 (274).
[34] Justin Heinermann, Oliver Kramer. Machine learning ensembles for wind power prediction[J] Renewable Energy, 2016 (89).
[35] Yifan Huang, Yu Lei, Xuedong Luo, Chao Fu. Prediction of compressive strength of rice husk ash concrete: A comparison of different metaheuristic algorithms for optimizing support vector regression[J]. Case Studies in Construction Materials, 2023 (18).
[36] Huixiang Liu, Qing Li, Dongbing Yu, Yu Gu. Air quality index and air pollutant concentration prediction based on machine learning algorithms[J]. Applied Science, 2019 (9).
[37] Hearst M A, Dumais S T, Osuna E. Support vector machines[J]. IEEE Intelligent Systems and their applications, 1998, 13(4): 18-28.
[38] Tianqi Chen, C. Guestrin. XGBoost: A scalable tree boosting system, in: Proc. ACM SIGKDD Int. Conf[J].Data Mining and Knowledge Discovery, 2016.
[39] Sonia Kahiomba Kiangala, Zenghui Wang. An effective adaptive customization framework for small manufacturing plants using extreme gradient boosting-XGBoost and random forest ensemble learning algorithms in an Industry 4.0 environment[J]. Machine Learning, 2021 (4).
[40] Freund Yoav, Schapire Robert Elias. A decision-theoretic generalization of on-line learning and an application to boosting[J]. Journal of computer and system sciences, 1997, 55(1): 119-139.
[41] Jianchang M, Anil K J. Artificial neural networks: A tutorial[J]. Computer (Long Beach Calif), 1996 (29).
[42] Min-Chang Kang, Doo-Yeol Yoo, Rishi Gupta. Machine learning-based prediction for compressive and flexural strengths of steel fiber-reinforced concrete[J]. Construction and Building Materials, 2021 (266).
[43] Rumelhart David E., Hinton Geofrey E. Hinton, Williams Ronald J. Williams. Learning representations by back-propagating errors[J]. Nature, 1986, 323(6088): 533-536.
[44] L. Breiman. Random forests[J]. Machine Learning, 2001 (45).
[45] Liaw Andy, Wiener Matthew. Classification and regression by random Forest[J]. R news, 2002, 2(3): 18-22
[46] Safavian S R, Landgrebe D. A survey of decision tree classifier methodology[J]. IEEE transactions on systems, man, and cybernetics, 1991, 21(3): 660-674.

[47] Umer Saeed, Sana Ulah Jan, Young-Doo Lee, Insoo Koo. Fault diagnosis based on extremely randomized trees in wireless sensor networks, Reliab[J]. Reliability Engineering and System Safety, 2021 (205).

[48] Khuong Le Nguyen, Hoa Thi Trinh, Thanh T. Nguyen, Hoang D. Nguyen. Comparative study on the performance of different machine learning techniques to predict the shear strength of RC deep beams: Model selection and industry implications[J]. Expert Systems with Applications, 2023 (230).

[49] M.A. Haque, B. Chen, A. Kashem, T. Qureshi, A.A.M. Ahmed. Hybrid intelligence models for compressive strength prediction of MPC composites and parametric analysis with SHAP algorithm, Mater[J]. Materials Today Communications, 2023 (35).

[50] Scott Lundberg, Su-In Lee. A unified approach to interpreting model predictions. In: Advances in Neural Information Processing Systems[C]. Neural Information Processing Systems, 2017 (32).

[51] I.U. Ekanayake, D.P.P. Meddage, Upaka Rathnayake. A novel approach to explain the black-box nature of machine learning in compressive strength predictions of concrete using Shapley additive explanations (SHAP)[J]. Case Studies in Construction Materials, 2022 (16).

[52] F. Ergen, Ö.H. Bettemir, Development of BIM software with quantity take-off and visualization capabilities[J]. Journal of Construction Engineering and Management, 2022 (5):01–14.

551

Appendix

	b(mm)	h_0(mm)	f_c(MPa)	f_{ec}(MPa)	f_{et}(MPa)	f_y(MPa)	f_{fd}(MPa)	ρ(%)	r(%)	M_u(kN·m)
Tan Chen	100	116	48.2	0	0	408	0	0.97	0	6.18
	100	116	48.2	38.8	2.4	408	0	0.97	25	7.17
	100	116	48.2	38.8	2.4	408	0	0.97	50	8.31
	100	116	48.2	38.8	2.4	408	0	0.97	75	7.63
	100	116	0	38.8	2.4	408	0	0.97	100	5.91
	100	116	48.2	0	0	408	0	1.95	0	10.31
	100	116	48.2	38.8	2.4	408	0	1.95	25	11.02
	100	116	48.2	38.8	2.4	408	0	1.95	50	13.6
	100	116	48.2	38.8	2.4	408	0	1.95	75	13.51
	100	116	0	38.8	2.4	408	0	1.95	100	11.82
	100	116	48.2	0	0	503	0	1.95	0	13.86
	100	116	48.2	38.8	2.4	503	0	1.95	25	13.37
	100	116	48.2	38.8	2.4	503	0	1.95	50	15.42
	100	116	48.2	38.8	2.4	503	0	1.95	75	15.81
	100	116	0	38.8	2.4	503	0	1.95	100	13.71
Xiao Feng	100	116	47	0	0	344	0	1.95	0	10.53
	100	116	47	40.6	2.4	344	0	1.95	25	10.9
	100	116	47	40.6	2.4	344	0	1.95	50	11.1
	100	116	47	40.6	2.4	344	0	1.95	75	12.2
	100	116	0	40.6	2.4	344	0	1.95	100	11.3
	100	118	47	0	0	0	1310	0.43	0	4.42
	100	118	47	40.6	2.4	0	1310	0.43	25	5.59
	100	118	47	40.6	2.4	0	1310	0.43	50	6.21
	100	118	47	40.6	2.4	0	1310	0.43	75	5.46
	100	118	0	40.6	2.4	0	1310	0.43	100	6.22
	100	118	47	0	0	0	1310	0.85	0	9.6
	100	118	47	40.6	2.4	0	1310	0.85	25	10.1
	100	118	47	40.6	2.4	0	1310	0.85	50	10.4
	100	118	47	40.6	2.4	0	1310	0.85	75	10.65
	100	118	0	40.6	2.4	0	1310	0.85	100	10.2
Biyuan Wang	150	166	47	0	0	408	0	0.45	0	9
	150	166	47	40.6	2.4	408	0	0.45	25	9.75
	150	166	47	40.6	2.4	408	0	0.45	50	11.25
	150	166	47	40.6	2.4	408	0	0.45	75	12
	150	166	0	40.6	2.4	408	0	0.45	100	12.5
	150	166	47	0	0	408	0	0.91	0	19.25
	150	166	47	40.6	2.4	408	0	0.91	25	19.5
	150	166	47	40.6	2.4	408	0	0.91	50	19.75
	150	166	47	40.6	2.4	408	0	0.91	75	20.5
	150	166	0	40.6	2.4	408	0	0.91	100	22.5
	150	168	47	0	0	0	1260	0.2	0	9.5
	150	168	47	40.6	2.4	0	1260	0.2	25	10.25
	150	168	47	40.6	2.4	0	1260	0.2	5	10.25
	150	168	47	40.6	2.4	0	1260	0.2	75	11.25
	150	168	0	40.6	2.4	0	1260	0.2	100	11.5
	150	168	47	0	0	0	1260	0.4	0	12
	150	168	47	40.6	2.4	0	1260	0.4	25	15.5
	150	168	47	40.6	2.4	0	1260	0.4	50	17.5
	150	168	47	40.6	2.4	0	1260	0.4	75	19.5

	150	168	0	40.6	2.4	0	1260	0.4	100	21.5
Linglong Pan	150	166	46.5	0	0	345	0	0.91	0	17.08
	150	166	46.5	40.6	2.4	345	0	0.91	25	18.63
	150	166	46.5	40.6	2.4	345	0	0.91	50	19.25
	150	166	46.5	40.6	2.4	345	0	0.91	75	19.12
	150	166	0	40.6	2.4	345	0	0.91	100	18.93
	150	167	46.5	0	0	410	0	0.31	0	6.31
	150	167	46.5	40.6	2.4	410	0	0.31	25	6.95
	150	167	46.5	40.6	2.4	410	0	0.31	50	7.23
	150	167	46.5	40.6	2.4	410	0	0.31	75	8.83
	150	167	0	40.6	2.4	410	0	0.31	100	10.51
	150	167	46.5	0	0	410	0	0.63	0	10.85
	150	167	46.5	40.6	2.4	410	0	0.63	25	12.11
	150	167	46.5	40.6	2.4	410	0	0.63	50	13.34
	150	167	46.5	40.6	2.4	410	0	0.63	75	13.02
	150	167	0	40.6	2.4	410	0	0.63	100	12.83
	150	166	46.5	0	0	503	0	0.91	0	21.34
	150	166	46.5	40.6	2.4	503	0	0.91	25	22.56
	150	166	46.5	40.6	2.4	503	0	0.91	50	22.95
	150	166	46.5	40.6	2.4	503	0	0.91	75	24.02
	150	166	0	40.6	2.4	503	0	0.91	100	22.56
Junyu Chen	150	167	47	0	0	408	0	0.63	0	11
	150	167	47	40.6	3	408	0	0.63	25	12
	150	167	47	40.6	3	408	0	0.63	50	13
	150	167	47	40.6	3	408	0	0.63	75	13
	150	167	0	40.6	3	408	0	0.63	100	13
	150	166	47	0	0	408	0	0.91	0	19.25
	150	166	47	40.6	3	408	0	0.91	25	19.5
	150	166	47	40.6	3	408	0	0.91	50	19.75
	150	166	47	40.6	3	408	0	0.91	75	20.5
	150	166	0	40.6	3	408	0	0.91	100	21.5
	150	166	47	0	0	340	1260	0.5	0	23
	150	166	47	40.6	3	340	1260	0.5	25	24
	150	166	47	40.6	3	340	1260	0.5	50	27.5
	150	166	47	40.6	3	340	1260	0.5	75	27.5
	150	166	0	40.6	3	340	1260	0.5	100	25
	150	167	47	0	0	408	1260	0.41	0	18
	150	167	47	40.6	3	408	1260	0.41	25	19.25
	150	167	47	40.6	3	408	1260	0.41	50	22
	150	167	47	40.6	3	408	1260	0.41	75	22
	150	167	0	40.6	3	408	1260	0.41	100	23
	150	166	47	0	0	408	1260	0.55	0	22
	150	166	47	40.6	3	408	1260	0.55	25	27.5
	150	166	47	40.6	3	408	1260	0.55	50	23
	150	166	47	40.6	3	408	1260	0.55	75	27.5
	150	166	0	40.6	3	408	1260	0.55	100	26
	150	167	47	0	0	408	1260	0.67	0	17.5
	150	167	47	40.6	3	408	1260	0.67	25	22
	150	167	47	40.6	3	408	1260	0.67	50	22.5
	150	167	47	40.6	3	408	1260	0.67	75	20
	150	167	0	40.6	3	408	1260	0.67	100	20
	150	166	47	0	0	408	1260	0.96	0	23.75

	150	166	47	40.6	3	408	1260	0.96	25	27.5
	150	166	47	40.6	3	408	1260	0.96	50	25.5
	150	166	47	40.6	3	408	1260	0.96	75	27.5
	150	166	0	40.6	3	408	1260	0.96	100	27.5
	150	166	47	0	0	503	1260	0.96	0	27
	150	166	47	40.6	3	503	1260	0.96	25	30.5
	150	166	47	40.6	3	503	1260	0.96	50	30
	150	166	47	40.6	3	503	1260	0.96	75	31
	150	166	0	40.6	3	503	1260	0.96	100	27.5
Zufa Jiang	140	160	0	45.2	5	0	2437	0.7	100	34.8
	140	160	0	45.2	5	0	2437	1.05	100	43.6
	140	153	0	45.2	5	0	2437	1.76	100	51.4
	140	160	0	45.2	5	0	2701	0.38	100	27.6
	140	160	0	45.2	5	0	2001	0.178	100	52.2
	140	160	0	45.2	5	0	1000	0.105	100	30.9
	140	160	0	45.2	5	406	0	0.105	100	23.46
	140	160	45.2	0	0	0	2437	0.105	0	36.26
	140	160	45.2	0	0	0	1000	0.105	0	25.83
Ren Hu	150	248	49.4	0	0	470	1660	4.89	0	96.2
	150	257	0	42.1	4	470	1660	1.84	100	45.96
	150	254	0	42.1	4	470	1660	2.69	100	70
	150	248	0	42.1	4	470	1660	4.89	100	117.7
	150	248	49.4	42.1	4	470	1660	4.89	30	105.4
	150	128	49.4	42.1	4	470	1660	9.45	30	44.9
	150	148	49.4	42.1	4	470	1660	8.19	30	53.5
	150	178	49.4	42.1	4	470	1660	6.81	30	68.9
	150	198	49.4	42.1	4	470	1660	6.12	30	78.9
	150	228	49.4	42.1	4	470	1660	5.32	30	94.4
	100	198	49.4	42.1	4	470	1660	9.187	30	69.2
	150	248	49.4	42.1	4	470	1660	4.89	16.7	102.1
	150	248	49.4	42.1	4	470	1660	4.89	43.3	113.5
	150	248	49.4	42.1	4	470	1660	4.89	56	105.6
	150	248	49.4	42.1	4	470	1660	4.89	70	104.5
	150	248	49.4	42.1	4	470	1660	4.89	83	101.5
	150	248	40	42.1	4	470	1660	4.89	30	92.5
	150	248	50	42.1	4	470	1660	4.89	30	106.1
	150	248	60	42.1	4	470	1660	4.89	30	110.5
	150	248	70	42.1	4	470	1660	4.89	30	124.9
	150	248	80	42.1	4	470	1660	4.89	30	133.1
Shuo Wang	150	264	31.25	0	0	0	910	0.571	0	21.3
	150	264	31.25	29.76	2.5	0	910	0.571	33	27
	150	264	31.25	29.76	2.5	0	910	0.571	67	27.6
	150	264	31.25	29.76	2.5	0	910	0.571	100	30.3
	150	264	31.25	0	0	0	910	0.85	0	24.3
	150	264	31.25	29.76	2.5	0	910	0.85	33	33.6
	150	264	31.25	29.76	2.5	0	910	0.85	67	36.3
	150	264	31.25	29.76	2.5	0	910	0.85	100	30.6
	150	264	43.5	29.76	2.5	0	910	0.57	33	30.6
	150	264	50.34	29.76	2.5	0	910	0.57	33	33.9